Available online at www.sciencedirect.com
SCIENCE DIRECT®
Acta Materialia 53 (2005) 1597–1609
Acta MATERIALIA
www.actamat-journals.com

Comparative study of grain-boundary migration and grain-boundary self-diffusion of [0 0 1] twist-grain boundaries in copper by atomistic simulations

B. Schönfelder [a], G. Gottstein [a,*], L.S. Shvindlerman [b]

[a] *Institut für Metallkunde und Metallphysik, RWTH Aachen University, Kopernikusstrasse 14, D-52056 Aachen, Germany*
[b] *Institute of Solid State Physics, Russian Academy of Sciences, Chernogolovka, Moscow 142432, Russia*

Received 26 November 2004; accepted 3 December 2004
Available online 5 January 2005

Abstract

Molecular-dynamics simulations were used to study grain-boundary migration as well as grain-boundary self-diffusion of low-angle and high-angle [0 0 1] planar twist grain boundaries (GBs) in copper. Elastic strain was imposed to drive the planar [0 0 1] twist GBs. The temperature dependence of the GB mobility was determined over a wide misorientation range. Additionally grain-boundary self-diffusion was studied for all investigated [0 0 1] planar twist GBs. A comparison of the activation energies determined shows that grain-boundary migration and self-diffusion are distinctly different processes. The behavior of atoms during grain-boundary migration was analyzed for all studied GBs. The analysis reveals that usually in absolute pure materials high-angle planar [0 0 1] twist GBs move by a collective shuffle mechanism while low-angle GBs move by a dislocation based mechanism. The obtained activation parameters were analyzed with respect to the compensation effect.

Keywords: Molecular-dynamics simulation; Twist-grain boundaries; Grain-boundary migration; Grain-boundary self-diffusion; Misorientation dependence

1. Introduction

Internal interfaces like grain boundaries (GBs) play an important role in the physical behavior of polycrystalline materials. Their ability to move constitutes the mechanism of microstructural change during annealing which causes recrystallization and grain growth. Moreover, GBs have high diffusivities and serve as fast diffusion paths, which becomes particularly noticeable at not so high temperatures when volume diffusion ceases.

In spite of the importance of GB migration and diffusion for microstructural evolution little is known about their atomic-level mechanisms. During the past 50 years many experiments have been conducted to investigate the basic properties of GBs, for instance the misorientation dependence of the GB energy, mobility, diffusivity, and basic concepts like the Read–Shockley model of low angle boundaries [1] or the compensation effect [2,3] evolved from these results. Regardless of these achievements there is virtually no theory of grain-boundary migration to date.

Recent computer simulations of GB migration on an atomic level were conducted and new concepts were introduced to obtain the key parameters of GB migration. Another aspect of GB behavior is possible structural transitions of GBs below the melting point. Recent results by Keblinski et al. [4] substantiate that certain GBs do change their structure with temperature.

* Corresponding author. Tel.: +49 241 802 6860; fax: +49 241 802 2608.
E-mail address: gottstein@imm.rwth-aachen.de (G. Gottstein).

1359-6454/$30.00
doi:10.1016/j.actamat.2004.12.010

Such structural transitions must have an impact on GB processes like GB self-diffusion and GB migration [4].

In early atomistic studies of GB motion [5–8] it was observed that GBs move even without any driving forces (DFs). Usually this was due to attractive forces on the GBs due to periodicity effects of the simulation box. A coupling of GB sliding and GB migration was found by Bishop [6–8] for different high-angle GBs as expected from the geometric theory of grain-boundary structure, but as evident from the experimental results of Babcock and Balluffi [9] the motion of secondary GB dislocations cannot account for the observed GB migration rates.

The first atomistic study on a curved GB system is due to Jhan and Bristowe [10] who studied migration of a GB with hemispherical geometry. It consisted of a planar twist GB with a protrusion of the shape of a hemisphere. The main finding of Jhan and Bristowe was a cooperative shuffle mechanism of GB migration which was also observed by Majid and Bristowe [11] in atomistic simulations and which was supported by experiments of Babock and Balluffi [9].

This concept is supported by direct experimental measurements of the motion of individual GBs in pure aluminium [12]. The measured activation enthalpy of grain-boundary migration can be substantially larger than the activation enthalphy for bulk self-diffusion [13]. Moreover, studies of grain-boundary motion under high hydrostatic pressure have shown that for $\langle 1\ 1\ 0\rangle$ tilt boundaries the activation volume of grain-boundary motion is three times larger than the atomic volume [13].

A constant DF concept on curved GB systems was presented by Upmanyu et al. [14] who utilized the curvature as DF on a U-shaped GB in a 2D atomistic simulation box. Various aspects of GB migration were studied by this approach like the misorientation dependence of GB mobility [15], the compensation effect [15] and vacancy emission of curved GBs during GB migration [16]. A method to realize a constant DF concept for planar GBs was given by Schönfelder et al. [17] where for the first time GB migration of a planar $\Sigma 29$ [0 0 1] twist GB due to an elastic DF was studied. This work serves here as the basis to study GB migration of various [0 0 1] twist GBs as also addressed previously [18].

2. Computational approach

2.1. Potential and MD box

In this work, atomistic GB migration simulations of planar [0 0 1] twist GBs in face-centered cubic (fcc) bicrystals are discussed. The utilized simulation method was molecular dynamics (MD) [19,20]. In our MD simulations a standard fifth-order Gear-predictor-corrector technique [20] was used to integrate the equations of motion of each atom. Throughout all simulations we applied 3D periodic boundary conditions, and all simulations were performed at constant temperature utilizing the Nose-Hoover-thermostat [21]. The time step was held constant during the simulations, $\Delta t = 1.84$ fs. For simplicity and also because the potential function has been widely used for GB simulations [22,23], an adapted Lennard–Jones (LJ) potential representing copper material was utilized.

The analytical expression for the used LJ potential is given by Eq. (1)

$$V^{\mathrm{LJ}}(r_{ij}) = 4\epsilon \cdot \left(\left(\frac{\sigma}{r_{ij}}\right)^{12} - \left(\frac{\sigma}{r_{ij}}\right)^{6} \right), \tag{1}$$

where r_{ij} represents the distance between atom, i, and atom, j. For the 3D LJ Cu potential used, the specific input parameters were $\sigma = 2.3151$ Å $= 0.905433 \cdot r_{\mathrm{NN}}$ and $\epsilon = 0.167$ eV with r_{NN} being the nearest neighbour distance. Here the specific value of σ is related to the minimum of the potential energy of an ideal crystal configuration assuming a certain cut off radius while ϵ determines the depth of the potential function and hence the bond strength.

$$V^{\mathrm{SF}}(r_{ij}) = V^{\mathrm{LJ}}(r_{ij}) - V^{\mathrm{LJ}}(r_{\mathrm{C}}) - (r_{ij} - r_{\mathrm{C}}) \cdot \frac{\mathrm{d}V^{\mathrm{LJ}}(r_{\mathrm{C}})}{\mathrm{d}r_{ij}}. \tag{2}$$

A shifted-force procedure according to Eq. (2) (see i.e. [20]) was applied with a cut-off radius of $r_{\mathrm{C}} = 1.49a_0$, where $a_0 = 3.616$ Å is the zero Kelvin lattice parameter of Cu, to avoid discontinuities in the energy and forces. The chosen r_{C} represents a cut off between fourth- and fifth-order nearest neighbours. These conditions gave a melting temperature $T_{\mathrm{m}} \approx 1250$ K, and a cohesive energy per atom $e_{\mathrm{coh}} = -1.037824$ eV/atom in 3D periodic ideal crystal simulations. It is noted that the prime reason for utilizing a LJ potential was to represent a typical fcc material rather than Cu in each and every detail. Relevant physical properties connected to the utilized 3D LJ potential obtained by ideal fcc crystal simulations are the temperature dependence of the lattice parameter [24], the temperature dependence of the elastic constants [25]. The temperature dependence of the lattice parameter, a, for the 3D LJ Cu potential could be represented by a second-order polynominal fit as given by $a(T) = a_0(1 + \alpha \cdot T + \beta \cdot T^2)$ with $\alpha = 2.0 \times 10^{-5}$ $(1/K)$ and $\beta = 1.8934 \times 10^{-8}$ $(1/K^2)$. The temperature dependence of the elastic constants was obtained by Jaszczak [25] for an ideal fcc crystal.

In this study only true CSL [0 0 1] planar twist GBs were studied. Fig. 1 shows schematically the MD box construction for all studied [0 0 1] twist GBs of this work. The GB plane normal was always parallel to the z direction of the MD simulation box coordinate system (x, y, z). With respect to a single crystal reference orientation grain A, which is underneath the sketched GB, is

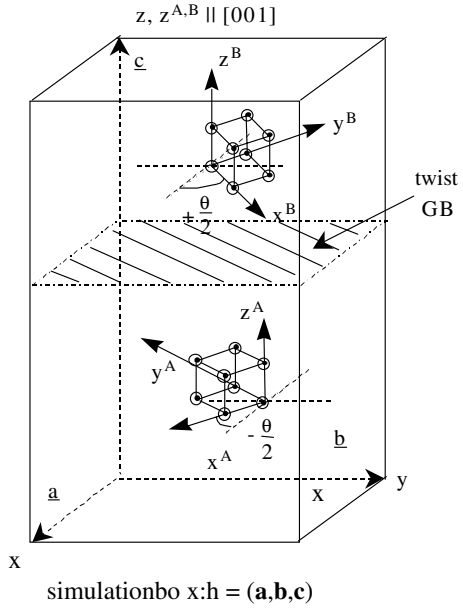

Fig. 1. Here a bicrystalline MD simulation box containing two grains labelled A and B for the case of an arbitrary [0 0 1] twist GB is shown. The direction of grain rotation and the primitive cells for a simple cubic material are illustrated in the figure as well. Note that both grains are symmetrically misoriented with respect to the MD simulation box coordinate system (x, y, z). The box vectors **a**, **b** and **c** that span out the simulation box are shown as well.

rotated $-\theta/2$ about the z direction of the MD box while grain B, which is above the GB, is rotated by $+\theta/2$. In this case the z-direction of the GB MD box coincides with the [0 0 1] direction of the cubic crystal lattice. Since 3D periodicity was applied, a second GB was present in the simulation box system along the z-direction of the box. Both GBs were identical. Overall the two grains had a misorientation relationship corresponding to a rotation by θ about the GB plane normal, namely [0 0 1].

The GB properties of the fully relaxed GB systems were obtained from lattice-statics simulations according to the steepest gradient method. For the [0 0 1] twist GBs at 0 K connected to the 3D LJ potential they are listed in Table 1.

2.2. Driving force and GB migration

Owing to the planar geometry of the studied GBs, there was no DF due to curvature. An elastic DF was utilized, i.e. a fixed elastic strain state was applied to the bicrystal simulation box in order to install different amounts of elastic energy in either of the two grains of the bicrystal. The underlying methodology had been worked out in detail by Schönfelder et al. [17] for the case of [0 0 1] twist GBs in cubic materials recently. Here only the relevant equations are given to compute the elastic DF and the necessary strain state to impose a constant DF on the system. Transformation of the strain tensor $\underline{\underline{\varepsilon}}$ which is to be applied to the MD simulation box into the principal cubic coordinate system of grains A and B and calculation of the difference between the elastic energy densities in grains A and B yields the elastic DF, p_{ela}.

$$p_{\mathrm{ela}} = E^{\mathrm{B}}_{\mathrm{ela}} - E^{\mathrm{A}}_{\mathrm{ela}} = \tfrac{1}{2} C_{ijkl}(\epsilon^{\mathrm{B}}_{ij}\epsilon^{\mathrm{B}}_{kl} - \epsilon^{\mathrm{A}}_{ij}\epsilon^{\mathrm{A}}_{kl}), \tag{3}$$

where the Einstein convention has been assumed.

For the [0 0 1] twist GBs in cubic materials following the MD box geometry shown in Fig. 1

$$p_{\mathrm{ela}} = -(2C_{4444} - C_{1111} + C_{1122}) \cdot \varepsilon^2 \cdot \sin(2\theta)$$
$$\text{when } \underline{\underline{\epsilon}} = \begin{pmatrix} \frac{\epsilon}{2} & \epsilon & 0 \\ \epsilon & -\frac{\epsilon}{2} & 0 \\ 0 & 0 & 0 \end{pmatrix}. \tag{4}$$

To determine and to track the position of the GBs throughout the MD simulations the so-called common-neighbour structural analysis (CNA) [26,27] method was utilized. Several criteria were applied to the atomistic data to distinguish true GB atoms from the rest. First, according to the CNA method, true ideal fcc atoms were determined in the system where each true ideal fcc atom could be recognized by its sharing of (4 2 1) triplets with its 12 nearest neighbours. Any atom

Table 1
General information on the [0 0 1] twist GBs

θ (°)	Σ	E_{GB} (J/m^2)	Inplane CSL cells	No. of (0 0 2) planes	Total no. of atoms	ΔV^{GB} (a_0)
43.60	29	0.716	1 or 4	80	2320 or 9280	0.12204
36.87	5	0.715	9	84 or 120	3780 or 5400	0.12080
28.07	17	0.700	4	84	5712	0.11623
22.62	13	0.677	4	84	4368	0.11144
16.26	25	0.625	2	84	4200	0.10350
12.68	41	0.582	1	110	4510	0.09801
8.80	85	0.490	1	84	7140	0.08517
6.03	181	0.404	1	72	13,032	0.07324

The table includes the misorientation angle θ, the GB energy E^{GB}, the x–y planar dimensions of the studied GB systems, namely the number of CSL cells within each (0 0 2) plane, the total number of (0 0 2) planes within the overall MD box, the total number of atoms in the MD simulation box, and the volume expansion of the GBs ΔV^{GB}.

that was not identified as a true ideal fcc atom was then considered as a potential GB atom. These non-ideal fcc atoms sometimes included bulk vacancies too and further data analysis was needed to rule those out. For this the system was sliced into slabs of (0 0 2) planes and a histogram of all non-fcc atoms was established. By analysing these histograms, the centers of mass of the GBs were calculated and their temporal evolution was tracked. This data analysis was applied on stored atomistic configurations and not during the MD simulation runs. The used storage intervals were one box every 1.84 ps. This described data analysis allowed one to track the GB position versus time. The GB velocity was obtained from a linear best data fit of GB position versus time.

The tools to identify GB migration mechanisms are quite limited. The dilemma is that the 3D atomic-level data are rather difficult to view in 3D. Usually a reduction to 2D plots can help to reveal the GB migration mechanism. This can be achieved by using projections along certain crystallographic directions. For [0 0 1] twist GBs this approach is less appropriate due to the overlay of bulk atomic positions of two grains in [0 0 1] projection.

Therefore, plots of single (0 0 2) planes were used to identify the GB migration mechanisms. This is based on the fundamental idea that at least at low temperatures the displacement field of atoms is dominated by in-plane movement of atoms. This was also found by Majid and Bristowe [11] for $\Sigma 5$ [0 0 1] twist GBs. They observed the formation of ledges by collective in-plane rotations of four atoms. The temporal evolution of the atomic arrangements in a specific (0 0 2) plane was recorded to identify the in-plane movement of the atoms. In order to obtain information on the migration mechanisms it is insufficient to plot only the instantaneous position of each atom in a (0 0 2) plane. The following scheme was used to obtain more information:

(1) Initially one attributes all atoms in a selected (0 0 2) plane to this plane. During the temporal evolution of the selected plane it is counted how many of the original atoms have remained in the plane and how many atoms have entered from neighbouring planes. In the simulations it was observed that the higher the temperature, the more atoms came from neighbouring planes.
(2) Next the in-plane displacement field of atoms within a chosen (0 0 2) plane should be characterized throughout the whole MD simulation. Hence, at each time step when the atomistic configuration of the selected (0 0 2) plane is analyzed, the instantaneous position of an atom was connected with its initial position by a line. This line identified the in-plane displacement vector of each atom. If an atom had left its original plane, its initial position was no longer connected to any atom's instantaneous position. If an atom had entered the selected (0 0 2) plane from a neighbouring plane, only its instantaneous position was plotted.
(3) The bond order with respect to NN atoms was analyzed to identify neighbours belonging either to orientation one, orientation two or neither of the two orientations. Each bond between atoms was analyzed with respect to the expected bond angle for either of the two orientations. The detected angles were allowed to deviate from the ideal ones by a few degrees to compensate the effect of thermal vibrations of the atoms. A color code was used to label the bonds. The number of ordered bonds was tracked as well.
(4) Finally the planar structure factor [28] was calculated to identify the long-range order within the selected (0 0 2) plane. This information was helpful to quantify the process of orientation change of the selected (0 0 2) plane, but it was only of minor help to identify the GB migration mechanism itself.

2.3. GB diffusion

The temporal evolution of the mean-square displacement (MSD) of atoms can be used to determine the diffusion coefficient, D, of various diffusive processes in atomistic systems.

In this study GB properties were of fundamental interest especially a comparison of the processes of GB migration and GB self-diffusion. The chosen calculation scheme was based on the MSD contribution of GB atoms arising from GB self-diffusion. Usually in literature rather restricted atomic systems were used to study GB self-diffusion [4,29,30] to suppress GB sliding. It is a common experience that GB sliding typically occurs under 3D periodic boundary conditions. For the studied GBs this was found very often. Nevertheless all studied GBs were simulated in such a way that GB sliding was still possible, since GB sliding, GB migration, and GB self-diffusion were conceived to always occur simultaneously. Hence in order to study real material behavior GB sliding was not a priori suppressed.

Since GB sliding occurred during almost every conducted GB simulation, a refined analysis of atomic displacements was necessary to determine only the diffusive GB MSD. Usually in the conducted MD simulations every 1000 time steps the position of each atom within the system was stored to be analyzed subsequently. Hence, the data analysis on atomic configurations was performed in time steps of usually 1.84 ps. The analysis procedure itself worked in two steps. In step one at time t the CNA method was used to classify atoms either as true fcc atoms or not. Any true fcc atom

was excluded from the GB MSD analysis at time t and its instantaneous position was kept as reference position for the following analysis at $t + \delta t$. Non-fcc atoms were evaluated to calculate the diffusive GB MSD. In order to separate GB sliding displacements from GB self-diffusion data, a threshold displacement of $0.35a_0$ was used. Any GB atom having a displacement less than $0.35a_0$ between $t-\delta t$ and t was considered non-diffusive and did not enter the calculation of the diffusive GB MSD at time t. Its position at time t was kept as the reference position for the following time step. Only displacements beyond the nearest-neighbour (NN)-distance were counted diffusive and used to calculate the GB diffusive MSD at time t. If considered diffusive the displacement of that atom was counted to the GB MSD and the position at time t was kept as the new reference position for the following time step. Accordingly, only the diffusive MSD of GB atoms was determined. Apart from GB sliding, GB migration events occurred during such simulations as well although no explicit DF had been introduced. Nevertheless the presented analysis scheme was able to separate atomic displacements due to GB migration and GB sliding from the diffusive GB displacement data too.

Once the GB diffusive MSD data was determined, the GB self-diffusion coefficient, D_{GB} was calculated from Eqs. (5) and (6)

$$\mathrm{MSD}(t,t_0) = \frac{\mathrm{SSD}(t,t_0)}{N_{\mathrm{GB}}} = \frac{1}{N_{\mathrm{GB}}}\sum_{j=1}^{N_{\mathrm{GB}}}(\mathbf{r}_j(t+t_0)-\mathbf{r}_j(t_0))^2, \tag{5}$$

$$D_{\mathrm{GB}} = \lim_{t\to\infty}\left\langle \frac{\mathrm{MSD}}{2\cdot\dim\cdot t}\right\rangle_{t_0}, \tag{6}$$

where SSD represents the summed-square displacement of all true GB atoms. The quantity dim defines the spatial dimension of the diffusive process which was considered here as three-dimensional because at high temperatures the diffusive jumps clearly become three-dimensional.

Eq. (5) implies that the diffusive GB MSD is normalized to the number of GB atoms, N_{GB}. Unfortunately, the definition of the GB region and its width as well as the number of GB atoms is not a simple and unambiguous task. In the following it will be shown that it is not necessary to normalize the GB MSD data directly to the number of GB atoms but rather to the GB area. Hence Eq. (5) serves as the starting point to derive the final equation to determine the GB self-diffusion coefficient.

N_{GB} needed to be quantified which could be achieved by approximating N_{GB} through the GB area A_{GB} the GB width, δ, and is the atomic volume of a single atom Ω_{fcc}. The number of GB atoms is given by

$$N_{\mathrm{GB}} \approx \frac{A_{\mathrm{GB}}\cdot\delta}{\Omega_{\mathrm{fcc}}}. \tag{7}$$

Furthermore the temporal evolution of the GB diffusive MSD and SSD data was expected to be linear in time, and so in Eq. (6) the average over $\langle\cdots\rangle_{t_0}$ became irrelevant for the calculation. Usually the average $\langle\cdots\rangle_{t_0}$ has to be taken over different time origins t_0. The final equation for the GB self-diffusion coefficient, D_{GB}, in this study was given by

$$\frac{\delta\cdot D_{\mathrm{GB}}}{\Omega_{\mathrm{fcc}}} = \lim_{t\to\infty}\frac{\sum_{j=1}^{N^{\mathrm{DGB}}}(\mathbf{r}_j(t)-\mathbf{r}_j(t_0=0))^2}{A_{\mathrm{GB}}\cdot 2\cdot\dim\cdot t} = \lim_{t\to\infty}\frac{\mathrm{SSD}}{A_{\mathrm{GB}}\cdot 2\cdot\dim\cdot t}. \tag{8}$$

Here N^{DGB} represents only the diffusive GB atoms according to the above mentioned selection scheme. Evidently D_{GB} cannot be obtained separately rather only data on $\frac{\delta\cdot D_{\mathrm{GB}}}{\Omega_{\mathrm{fcc}}}$ were determined. The expression $\frac{\delta\cdot D_{\mathrm{GB}}}{\Omega_{\mathrm{fcc}}}$ was obtained by a plot of SSD versus time where the slope multiplied by the factor $\frac{1}{2\cdot\dim\cdot A_{\mathrm{GB}}}$ gives $\frac{\delta\cdot D_{\mathrm{GB}}}{\Omega_{\mathrm{fcc}}}$.

3. Results

3.1. GB migration

In our previous study of GB migration of [0 0 1] planar twist GBs [18] we determined the temperature dependence of GB mobility for various [0 0 1] planar GBs by utilizing the elastic DF concept. Grain-boundary migration is a thermally activated process and thus follows an Arrhenius dependency

$$v = mp, \tag{9}$$

$$m = m_0\ \exp\left(-\frac{Q_{\mathrm{GBM}}}{kT}\right). \tag{10}$$

Fig. 2 summarizes the determined temperature dependence of GB mobility for various [0 0 1] planar twist GBs. A linear regression on the GB mobility data yielded the activation parameters, namely the activation enthalpy, Q_{GBM}, and the GB mobility pre-exponential factor, m_0, as listed in Table 2. The activation enthalpy of GB migration Q_{GBM} is plotted versus the misorientation angle θ in Fig. 3. The Σ29 GB results are special in the sense that a low temperature and a high temperature regime were found as indicated in Fig. 2 by two sets of linear best data fits. For six further twist GBs only a single regime was observed, and the activation parameters compared best to the low temperature regime of the Σ29 boundary. The migration of the Σ181 twist GB was found to proceed athermally, i.e. the mobility was virtually independent of temperature. It is noted in this context that the Σ181 GB migration results were obtained from computations with OCDF [18].

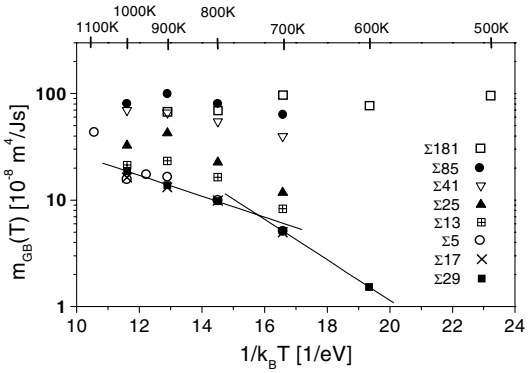

Fig. 2. Arrhenius plot of GB mobility for the studied [0 0 1] twist GBs. The temperature dependence of GB mobility yields the activation parameters, namely the activation enthalpy Q_{GBM}, as well as the pre-exponential factor m_0. The determined data for each GB is listed in Table 2. For the Σ29 GB a high and a low temperature regime were found as represented by the two different linear best data fits.

Table 2
GB migration activation parameters of the studied [0 0 1] twist GBs

GB plane	θ (°)	Σ	Q_{GBM} (eV)	$m_0((10^{-6})m^4/Js)$
(0 0 1)	43.60	29	0.438	73.06
	43.60	29	0.226 ± 0.008	2.57
(0 0 1)	36.87	5	0.319 ± 0.001	10.21
(0 0 1)	28.07	17	0.267 ± 0.040	4.32
(0 0 1)	22.62	13	0.284 ± 0.030	9.39
(0 0 1)	16.26	25	0.346 ± 0.020	35.94
(0 0 1)	12.68	41	0.109 ± 0.030	2.19
(0 0 1)	8.80	85	0.121 ± 0.010	4.69
(0 0 1)	6.03	181	0.0	0.80

The results were obtained for the LJ potential with 3D periodic BC and an elastic DF. The only exception is the result of the Σ181 GB which was obtained for the LJ potential but for the so-called orientation-correlated DF [18].

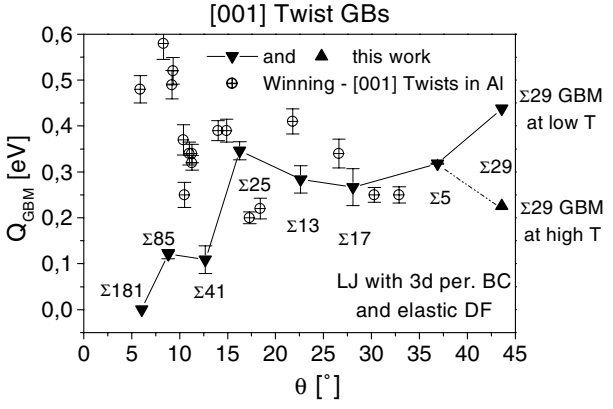

Fig. 3. Misorientation dependence of the activation enthalpy of GB migration of the studied [0 0 1] twist GBs. The shown data represent the results of the LJ 3D periodic BC simulations in the presence of an elastic DF. Additionally experimental data of planar [0 0 1] twist GBs in Al according to Winning [31] are plotted as well.

A clear distinction between high-angle and low-angle GBs was reflected by the GB migration activation parameters. A low GB migration enthalpy for the two true low-angle twist GBs, namely the Σ41 and Σ85, of about 0.12 eV characterized the behavior of these low-angle GBs. For the Σ181 twist GB even thermally non-activated GB migration was found according to the computed GB mobility data in the temperature from 500 K up to 900 K. The low-angle twist GBs consisted of discrete screw dislocation networks that remained stable throughout the studied temperature range as demonstrated for the Σ85 twist GB at 1000 K in Fig. 4. The discrete cores of the screw dislocations of the low-angle twist GBs were identified by utilizing the CNA scheme which showed that the crystal lattice does continue smoothly across the GB region outside of the screw dislocation cores in the boundary. The structural analysis

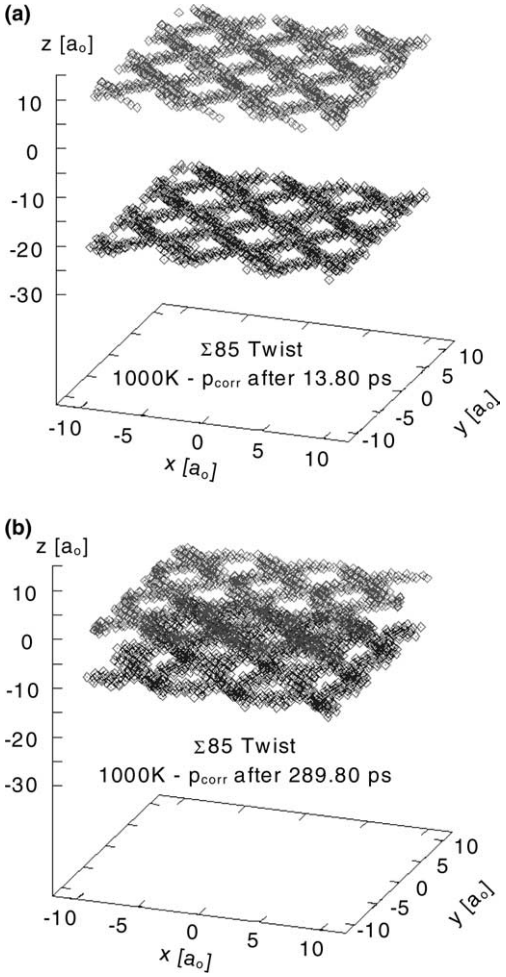

Fig. 4. 6.03° [0 0 1](Σ85) twist GB – screw dislocation network during GB migration at 1000 K and a DF of 0.0018 eV/atom. Here the CNA method was utilized to identify only non-ideal fcc atoms. These atoms form the screw dislocation network of the two present GBs and can be followed with time. In order to facilitate identification of the screw dislocation network the original MD cell was repeated periodically within the (0 0 2) plane.

revealed that the migration mechanism of low-angle twist boundaries was linked to a movement of the screw dislocation network itself. In contrast the high-angle twist GBs moved in the low temperature regime by collective shuffle mechanisms which were usually in-plane displacements. At elevated temperatures, an out-of-plane component entered into the migration mechanism which might be the cause for the change of GB migration mechanism as reflected by the drop of GB mobility above 900 K.

The obtained activation parameters lend themselves to an analysis with respect to the compensation effect. The compensation effect predicts a linear relationship between the activation enthalpy and the logarithm of the pre-exponential factor for thermally activated processes, i.e. for grain-boundary mobility

$$Q_{\mathrm{GBM}} = \alpha + \beta \ln m_0 \text{ with } \beta = k_{\mathrm{B}} T_{\mathrm{C}}, \tag{11}$$

which defines the compensation temperature T_{C}. Fig. 5 shows the compensation plot of the computed GB migration activation parameters of the studied [0 0 1] twist GBs. Two data sets seem to exist that are associated with either low-angle and high-angle [0 0 1] twist GBs. The found compensation temperatures seem reasonable. The low-angle twist GBs have a higher T_{C} compared to high-angle GBs. Due to the dislocation structure of low-angle twist GBs T_{C} is expected to be close to the melting temperature. The lower T_{C} for the high-angle twist GBs might be related to a possible change of the activation enthalpy as observed for the $\Sigma 29$ twist GB.

3.2. GB self-diffusion

From the temporal evolution of the diffusive SSD for each of the studied [0 0 1] twist GBs, the GB self-diffusion coefficients were determined. In Figs. 6 and 7 the diffusive GB SSD data was normalized to twice the GB area, $2 \cdot A_{\mathrm{GB}}$, in order to be representative for the later determination of the GB self-diffusion coefficient D_{GB}. To use twice the GB area was necessary since two [0 0 1] twist GBs were present in the simulation box because of the applied 3D periodic boundary conditions.

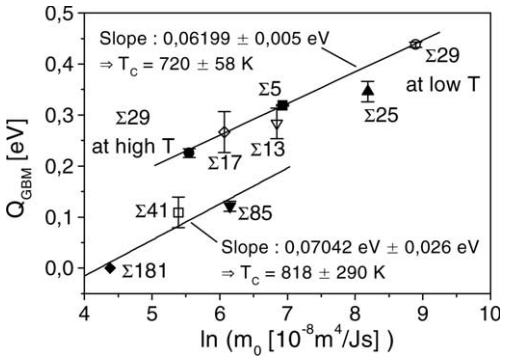

Fig. 5. Compensation plot of the GB migration activation parameters of the studied [0 0 1] twist GBs.

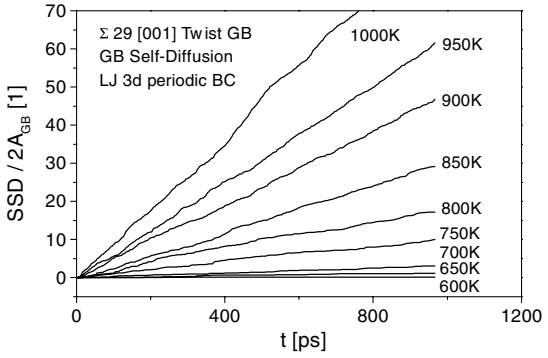

Fig. 6. Total diffusive SSD per GB area of the $\Sigma 29$ [0 0 1] 43.60° twist GB at different temperature.

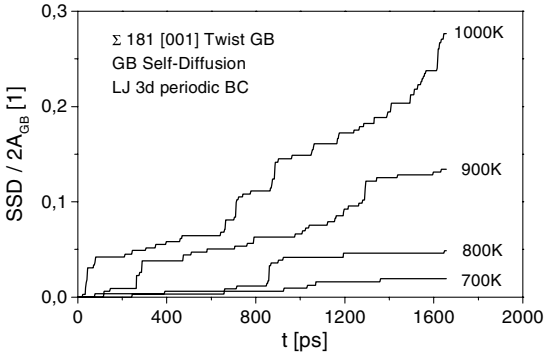

Fig. 7. Total diffusive SSD per GB area of the $\Sigma 181$ [0 0 1] 6.03° twist GB at different temperature.

At intermediate and high temperatures the diffusive jumps of atoms occurred no longer exclusively in-plane but very often out-of-plane. Also, the GB self-diffusion coefficient can only be determined as a product with the GB width δ which is temperature dependent as was shown by Keblinski et al. [4] and also found in this work. Since in most simulation runs GB migration events occurred most likely related to interaction of the two existing GBs, no attempt was made to determine the GB diffusional width itself.

Fig. 8 presents the GB self-diffusion data of the $\Sigma 29$ twist GB. The data is representative for the studied high-angle twist GBs since it exhibits one important aspect. For the $\Sigma 29$ and $\Sigma 5$ twist GBs we found that a low temperature and a high temperature regime existed for GB self-diffusion and GB migration. This is best seen for the GB self-diffusion data of the $\Sigma 29$ twist GB in Fig. 8. This behavior is in agreement with work of Keblinski et al. [4] who reported such behavior for high energy twist and tilt GBs as well. The high temperature activation enthalpy amounted to about half of the low temperature value.

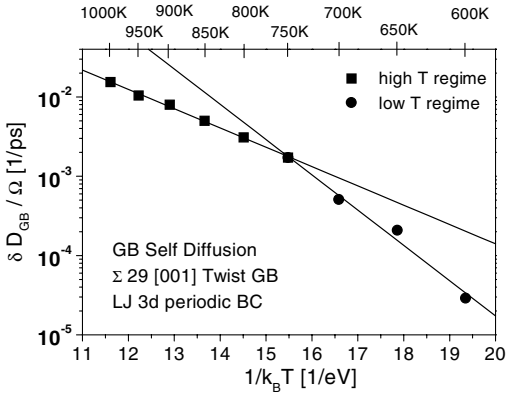

Fig. 8. Arrhenius plot of the GB self-diffusion data of the Σ29 [0 0 1] twist GB. Here the results of the temperature range 600–1000 K are given.

The determined temperature dependence of the GB diffusion coefficient D_{GB} is presented in an Arrhenius plot in Fig. 9. From a linear fit of the data the activation parameters for GB diffusion of these [0 0 1] twist GBs, namely the GB self-diffusion enthalpy and the GB self-diffusion pre-exponential factor were determined (Table 3) (see Figs. 10, 11).

Comparing the data of this work and the data by Nomura and Adams [30], a similar orientation dependence of the activation enthalpy was observed, i.e. the activation energy of self-diffusion was found to decrease with decreasing misorientation angle. A more detailed analysis of the data demonstrated that for the two low-angle twist GBs with lowest misorientation, namely Σ181 and Σ85, the activation enthalpies again increase with decreasing twist angle. We surmise that for even smaller twist angles the activation enthalpy will rise further or at least stay on a rather high level. In the limit of zero misorientation the volume self-diffusion activation enthalpy of 1.97 eV limit must be found, of course.

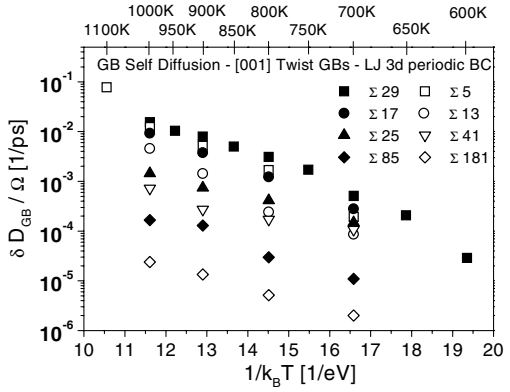

Fig. 9. Arrhenius plot of the GB self-diffusion data of the [0 0 1] twist GBs. The simulations were done for the LJ potential with 3D periodic BC and in the presence of no DF.

Table 3
GB self-diffusion activation parameters of the studied [0 0 1] twist GBs for the LJ potential utilizing 3D periodic BC

GB plane	θ (°)	Σ	Q_{GBD} (eV)	$\ln(\frac{\delta \cdot D^0_{GB}}{\Omega}[\frac{1}{ps}])$
(0 0 1)	43.60	29	1.023 ± 0.086	9.518
	43.60	29	0.560 ± 0.014	2.342
(0 0 1)	36.87	5	1.042	8.757
	36.87	5	0.684 ± 0.007	3.560
(0 0 1)	28.07	17	0.701 ± 0.030	3.464
(0 0 1)	22.62	13	0.816 ± 0.097	3.949
(0 0 1)	16.26	25	0.446 ± 0.020	−1.376
(0 0 1)	12.68	41	0.252 ± 0.016	−4.979
(0 0 1)	8.80	85	0.585 ± 0.081	−1.727
(0 0 1)	6.03	181	0.507 ± 0.020	−4.735

The data shown relates to MD finite temperature simulations without any DF.

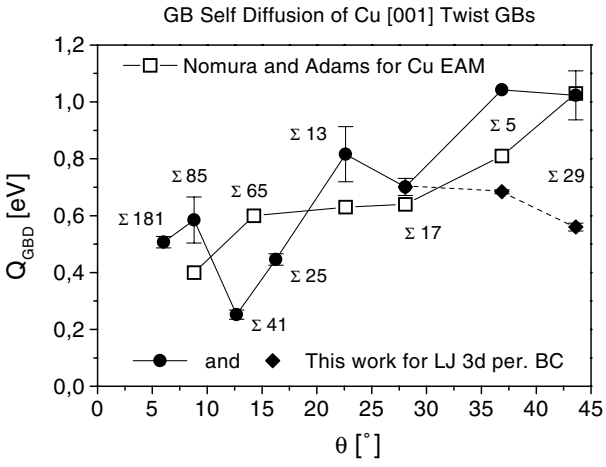

Fig. 10. Misorientation dependence of the activation enthalpy of GB self-diffusion of the studied [0 0 1] twist GBs. The data shown represent the results of the LJ 3D periodic BC simulations of this work and as a reference the results by Nomura [30].

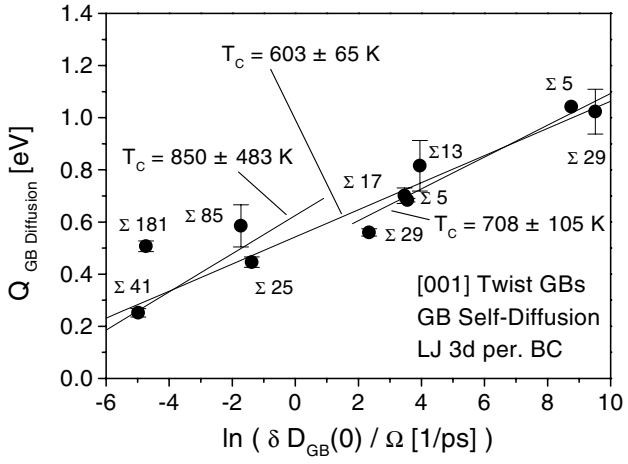

Fig. 11. Compensation plot of the GB self-diffusion data for the studied [0 0 1] twist GBs. Three linear data fits were done. One data fit of the overall data yielding 605 K for the compensation temperature, second a data fit of only the high-angle GB data yielding 708 K and finally a fit of only the low-angle GB data yielding 850 K.

Another interesting aspect were the low and high temperature GB self-diffusion regimes of the Σ29 and Σ5 twist GBs. The low temperature data of the Σ29 GB coincided with the Nomura and Adams data [30] perfectly well. Bearing in mind that the data of [30] related to an EAM potential this fact was probably only coincidental. In addition to the presented LJ data of this work further studies were conducted utilizing a Cu EAM Doyama potential [32] which are not presented in this work. Still the results of the EAM Doyama and the LJ potential for the Σ5 illustrate that the activation enthalpy derived from the LJ and EAM potentials do not differ dramatically. Therefore the Σ29 and Σ5 activation enthalpies were comparable with the data of Nomura and Adams. Another GB self-diffusion data analysis was performed on moving GBs driven by explicit DFs. It proved that GB self-diffusion remained almost identical for stationary and moving GBs. This is confirmed by recent experimental work [33,34] and hence adds further confidence in the used data analysis of this work. To underline this statement, the GB self-diffusion data for 950 and 1000 K of the Σ5 [0 0 1] twist GB in the stationary and moving case is presented in Table 4 for 950 and 1000 K. The data reveals that GB self-diffusion via vacancies remains the same for non-driven and driven GBs. No effect of the magnitude of the used DF on the GB self-diffusion data was found.

The GB self-diffusion activation data was also analyzed with respect to the compensation effect. The data seemed to distinguish between low-angle and high-angle GBs. This is best exemplified by the Σ85 data. For the Σ181, Σ85, Σ41 and Σ25 twist GBs, the quantity $\delta \cdot D_{GB}(0)/\Omega$, is much smaller than for the high-angle GBs. At first glance it seems that even the overall data can be fitted quite well by a linear regression. What raises some doubts is the fact that the activation enthalpy of the Σ85 boundary is rather high but $\delta \cdot D_{GB}(0)/\Omega$ seems rather low compared to the Σ5 and Σ17 data. This is especially true in view of the spread of the Σ29, Σ5, Σ17 and Σ13 activation enthalpy data which have similar $\delta \cdot D_{GB}(0)/\Omega$ values but are distinctly different from $\delta \cdot D_{GB}(0)/\Omega$ values of the Σ85 GB. Furthermore the overall linear fit finds 603 K as the compensation temperature. This temperature is understood to be related to a structural transition of the GBs [3]. The self-diffusion data of the Σ29 and Σ5 GBs suggest that they undergo a structural transition in the temperature range of 700–750 K. Including an uncertainty of 65 K the temperatures are at least comparable. According to the findings of Keblinski et al. [4], it is expected that the transition temperature of low-energy GBs and therefore low-angle twist GBs should be much higher than for random high-angle GBs. This suggests that the current low-angle and high-angle data form two separate data sets which need to be fitted independently. Corresponding fits of the low-angle and high-angle GB data yield compensation temperatures of 850 and 708 K, respectively. For the low-angle GB fit one notes a relative large error bar of 483 K. In general, the data is in agreement with the compensation effect, and the compensation temperature roughly agrees with the structural transition temperature of low- and high-angle GBs.

3.3. GB structure

In order to assess how ordered or disorded the GBs remain at elevated temperatures the angular distribution of the GB diffusion displacement vectors was analyzed. Such an analysis gives some insight into the question whether or not the GBs undergo structural transitions within the investigated temperature regimes [4]. The data presented in Figs. 12–15 represent the normalized angular distribution of diffusional GB jumps of at least the nearest neighbors distance. To perform such an analysis, first the CNA method was applied to identify the GB atoms. Then the displacement vectors had to be analyzed. Since GB sliding might interfere with the analysis scheme, an updating scheme of the reference position of each GB atom had to ensure that only diffusive GB

Table 4
GB self-diffusion coefficient determined from GB migration simulations of the Σ5 [0 0 1] twist GB at 950 and 1000 K

T (K)	p_{corr} (0.001 eV/atom)	$\delta D_{GB}/\Omega$ (1/ps)
950	0.00	0.0086368
950	3.20	0.0093457
950	6.38	0.0086679
1000	0.00	0.0143417
1000	3.15	0.0137255
1000	6.21	0.0137216

Here the results of simulations in the presence of an orientation-correlated DF, p_{corr}, are presented. For simulation runs at fixed temperature but different DFs, the GB diffusion coefficient remains the same. No systematic effect of the magnitude of the DF is observed on the GB diffusion coefficient.

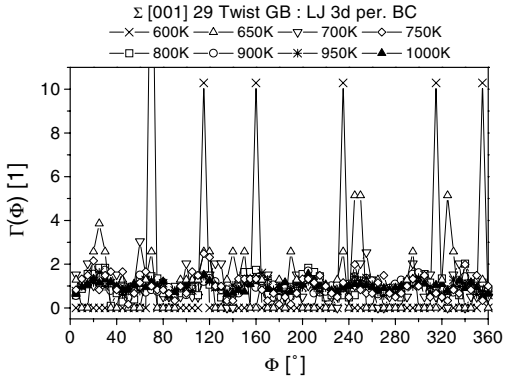

Fig. 12. Angular distribution of the diffusion jump vectors of the Σ29 [0 0 1] 43.60° twist GB at different temperatures.

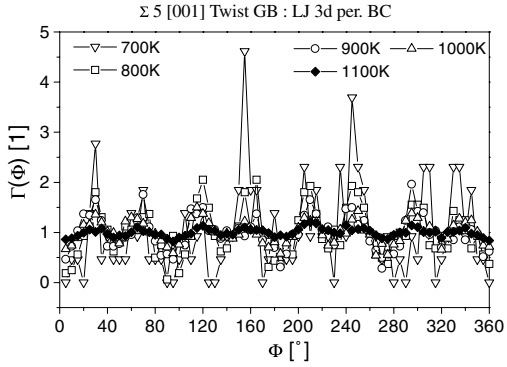

Fig. 13. Angular distribution of the diffusion jump vectors of the Σ5 [0 0 1] 38.87° twist GB at different temperatures.

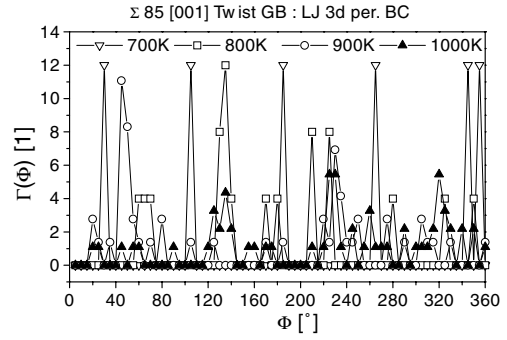

Fig. 14. Angular distribution of the diffusion jump vectors of the Σ85 [0 0 1] 8.80° twist GB at different temperatures.

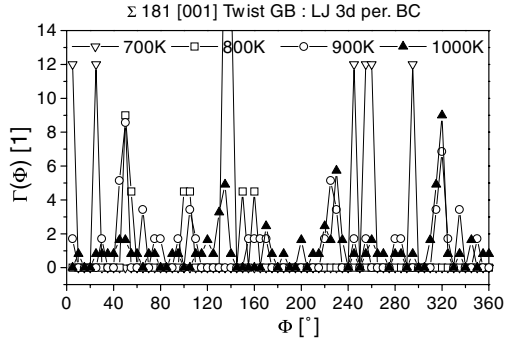

Fig. 15. Angular distribution of the diffusion jump vectors of the Σ181 [0 0 1] 6.03° twist GB at different temperatures.

jumps were oriented for their angular distribution. Once a jump was identified, it was examined with respect to its angular coordinate within the (0 0 2) plane. For this the jump vectors were projected onto the (0 0 2) plane and the jump angle was determined. The reference coordinate system for this analysis was the x–y simulation box coordinate system. For a complete MD run, all jump events and the sum of their angular distributions $\gamma(i)$ were represented in a histogram containing 72 classes of 5°. In order to normalize the angular histogram, the data of each class was normalized to

$$\Gamma(i) = (72 \cdot \gamma(i)) \Big/ \left(\sum_{i=1}^{72} \gamma(i) \right).$$

According to this normalization, an isotropic uniform angular distribution would have the value 1 for each of the 72 angular classes. Usually at low temperatures the GBs will have some structural order which has to be reflected in the diffusional data.

The analysis relies on the fact that discrete single GB diffusional jumps can be identified within the system. In the conducted MD simulations only after every 1000 time steps the position of all atoms in the system was stored. For high temperatures this means that not every single jump event can be identified, since numerous jump events can have occurred within the time range of a 1000 time steps. Nevertheless the approach is capable of identifying diffusional GB jump events and yields solid data on their angular distribution. From the angular distribution two main conclusions can be drawn:

(1) All high-angle GBs, especially the Σ29 and Σ5, seemed to undergo a structural transition far below the melting temperature. Such a transition is marked by the effect that a crystalline structure causes discrete peaks in the histogram, i.e. at discrete jump angles, while a loss of crystallinity is reflected by a tendency to a uniform distribution. Although the highest temperature profiles were not ideal and showed the characteristics of an underlying crystal structure of the GB, they tended to approach a uniform distribution. The degree of loss of GB structure, however, cannot be judged only on the basis of the angular distribution data.
(2) The studied low-angle GBs seemed to remain crystalline throughout the studied temperature range. The thermal weakening of the GB structure was less pronounced than in the case of high-angle [0 0 1] twist GBs.

4. Discussion

4.1. GB migration mechanism

The simulations revealed several GB migration mechanisms:

(1) Collective shuffle mechanism of four atoms for the Σ29, Σ5 and Σ17 GBs.
(2) Dislocation based mechanism for the Σ41, Σ85 and Σ181 GBs.
(3) Neither of the two mechanisms or hard to identify for Σ13 and Σ25 GBs.

The Σ29, Σ5 and Σ17 twist GBs at least at low and intermediate temperatures moved by a collective shuffle mechanism. The elementary act of the collective shuffle mechanism is a cooperative four atom movement. Majid and Bristowe [11] were the first to report a shuffle mechanism for the Σ5 [0 0 1] twist GB. Jhan and Bristowe [10] considered a hemispherical GB geometry and showed also a local shuffle mechanism to occur. These shuffles generally proceeded from the periphery of the ledge to its center.

The temperature range (300 K for Σ5, 500 K for Σ13, Σ17 and Σ29) investigated by Jhan and Bristowe was rather low compared to the temperatures studied in this work. The four atom shuffle could be easily detected by Jhan and Bristowe since the data analysis at low temperatures is much simpler than at elevated temperatures. At higher temperatures, the grains tend to vibrate or slide which makes the data analysis more complicated.

The migration of the Σ41, Σ85 and Σ181 twist GBs was found to be connected to the motion of their screw dislocation networks which can be characterized as follows:

(a) The GB structure in the studied temperature range (700–1000 K) consisted of a discrete network of screw dislocations. This network was even present at the highest applied temperatures.
(b) Normally no jumps of atoms accross the GB were observed during GB migration even at the highest studied temperatures. This shows that the GB migration mechanism was predominantly confined to each (0 0 2) plane. This behavior is quite different from high-angle twist GBs at elevated temperatures.
(c) GB sliding increased with rising twist angle. The Σ41 (12.7° twist GB still shows some tendency to GB sliding, but its magnitude is far less than for the Σ5 (36.9°) twist GB. This is attributed to an extension of the ideal crystal regions between the structured dislocations with decreasing twist angle. Also no explicit DF was imposed on the screw dislocation network to cause GB sliding.
(d) The final displacement field found in each (0 0 2) plane after a GB had swept the plane was dominated by in-plane displacements that were linked to the GB screw dislocation cores. The atoms moved in a cooperative manner. The largest displacement vectors were in the range of a NN distance or less. Even at the highest temperatures studied the discrete screw dislocation network of the low-angle twist GBs prevailed, and even when the approaching GBs came very close, this situation did not change. This demonstrates that the low-angle twist GBs behaved exactly like a discrete screw dislocation network in an fcc system without impurities. This finding helps to rationalize that the found activation enthalpies of the low-angle twist GBs are very low, even low compared to the studied [0 0 1] high-angle twist GBs in this work. Also, it explains the drop in activation enthalpy observed in the transition from high-angle [0 0 1] twist to low-angle twist GBs.

4.2. Comparison of grain-boundary migration and grain-boundary diffusion

Owing to a lack of reliable data on grain-boundary mobility it is frequently assumed that GB migration and GB diffusion involve the same mechanisms so that the activation energies are essentially identical. The computed activation enthalpies of GB self-diffusion of each GB and volume self-diffusion are listed in Table 5 namely $r_{\mathrm{vac}}^{\mathrm{GBD}} = \frac{Q_{\mathrm{GBD}}}{Q_{\mathrm{vac}}}$ and $r_{\mathrm{GBD}}^{\mathrm{GBM}} = \frac{Q_{\mathrm{GBM}}}{Q_{\mathrm{GBD}}}$. From these data we can draw the following conclusions:

(a) The computed GB self-diffusion activation enthalpy for the Σ29 and Σ5 twist GBs in the low temperature regime were about half the value for volume self-diffusion via mono-vacancies. The other listed data in Table 5 of $r_{\mathrm{vac}}^{\mathrm{GBD}}$ range from 0.128 to 0.414 depending on the misorientation angle of the GB. Generally $r_{\mathrm{vac}}^{\mathrm{GBD}}$ is assumed to be approximately 0.5.

Table 5
Scaling behavior of the found GB activation enthalpies of the studied [0 0 1] twist GBs for the LJ potential

GB plane	θ (°)	Σ	$Q_{\mathrm{GBD}}/Q_{\mathrm{vac}}$ [1]	$Q_{\mathrm{GBM}}/Q_{\mathrm{GBD}}$ [1]	$Q_{\mathrm{GBM}}/Q_{\mathrm{fus}}$ [1]
(0 0 1)	43.60	29	0.519	0.428	3.4
	43.60	29	0.284	0.404	1.7
(0 0 1)	36.87	5	0.528	0.306	2.5
	36.87	5	0.347	0.466	–
(0 0 1)	28.07	17	0.355	0.381	2.1
(0 0 1)	22.62	13	0.414	0.348	2.2
(0 0 1)	16.26	25	0.226	0.776	2.7
(0 0 1)	12.68	41	0.128	0.433	0.8
(0 0 1)	8.80	85	0.297	0.207	0.9
(0 0 1)	6.03	181	0.257	0.000	0.0

Here the activation enthalpy of volume self-diffusion via mono-vacancies in a fcc system modelled by the used LJ potential of this work with 3D periodic BC is $Q_{\mathrm{vac}} = 1.972$ eV. Further Q_{GBD} represents the GB self-diffusion enthalpy as determined in this work for each GB and Q_{GBM} is the GB migration enthalpy. Finally Q_{fus} is the latent heat of fusion as determined in [17] and reads $Q_{\mathrm{fus}} = 0.13$ eV.

(b) The r_{GBD}^{GBM} values range from 0.207 to 0.776 depending on the misorientation angle of the GB. Roughly speaking the ratio is one third to one half. This clearly demonstrates that GB migration and GB self-diffusion are distinctly different processes. The conclusion is supported by the results of the GB migration mechanisms discussed in Section 4.1, for instance for the studied high-angle [0 0 1] twist GBs a cooperative four atom shuffle mechanism was identified as the key element which was quite different from the GB diffusion mechanims.

This result is also supported by the findings of Merkle and Thompson [35] who conducted atomic resolution TEM experiments to observe in situ grain-boundary motion. They reported a cooperative shuffle process as the dominant migration mechanism. Winning [31] studied the motion of planar [0 0 1] low- and high-angle twist GBs in Al which were driven by an applied shear stress. Although the studied GBs were non-CSL GBs, still the experimental data lend themselves for a data comparison. It was observed experimentally that high-angle curved tilt GBs had a higher GB migration enthalpy than the same planar tilt GBs. Furthermore, it was observed that planar [0 0 1] tilt GBs had a higher activation enthalpy than [0 0 1] twist GBs. Of course, the level of purity influenced to some extent the magnitude of the GB migration activation enthalpy. The data of this study revealed that the computed GB migration enthalpies of the high-angle GBs were comparable to experiment. Since in Al the bulk self-diffusion enthalpy is 1.29 eV and in Cu 2.01 eV, the experimental activation data of a Cu material would be expected to be by about 35% larger than the Al data. For the low-angle GBs, the mobility data agreement is poor. The difference may be due to purity effects. Impurities may not only exert a drag on the boundary but may affect the core structure of the dislocations as well (e.g. dissociation) and, therefore, modify the migration mechanism of the dislocation network. In contrast, the screw dislocation network of the simulated low-angle GBs will behave as perfect screw dislocations which may explain the extremely low activation enthalpies.

Upmanyu et al. [15] conducted 2D MD simulations for an fcc model material. Only (1 1 1) planes could be modelled, and a U-shaped GB geometry was considered. In their work the energy unit that determined the strength of all energy terms was given by the input parameter ϵ of the LJ potential. Due to the 2D atomistic system size, the GB becomes a line defect. The studied GBs were in the vicinity of the $\Sigma 13$ and $\Sigma 7$ [1 1 1] tilt GB. They found minimum and maximum GB migration enthalpies of $Q_{min} = 0.302\epsilon$ and $Q_{max} = 0.456\epsilon$, respectively. For a direct comparison with the GB migration enthalpies found in this work the respective LJ ϵ value has be used to compare the data. In our work $\epsilon = 0.167$ eV, hence the minimum and maximum GB migration enthalpies obtained by Upmanyu et al. would be $Q_{min} = 0.050$ eV and $Q_{max} = 0.076$ eV, respectively, which is much smaller than the data found in this study. The small activation energy found by Upmanyu et al. is likely due to the 2D atomistic geometry.

5. Summary

Grain-boundary motion and grain-boundary diffusion was studied by MD simulations. An elastic DF was applied to planar [0 0 1] twist GBs to cause continuous GB migration. GB mobilities were extracted from the simulations. The GB mobility data followed an Arrhenius relationship. The activation enthalpies found for GB migration of high angle [0 0 1] twist GBs were slightly smaller than experimental reference data [18,31]. A different behavior was found for the studied low-angle [0 0 1] twist GBs in comparison to both high angle boundaries and experimental data. This is attributed to structural and chemical effects. All studied [0 0 1] twist GBs were also investigated with respect to GB self-diffusion. Good agreement of the activation enthalpy data of this work with the study by Nomura and Adams [30] was found. The GB self-diffusion activation enthalpies found in this work at a high temperature regime, however, clearly deviated from the Nomura and Adams data owing to the fact that Nomura and Adams had investigated the very low temperature regime.

The found activation enthalpies of GB migration and GB self-diffusion prove that GB migration can not be understood in terms of GB self-diffusion. Rather the GB migration mechanism of true high-angle GBs was found to be dominated by a collective shuffle mechanism of four atoms, which confirms findings reported by Bristowe and coworkers [10,11]. For the studied low-angle twist GBs, a dislocation based motion mechanism was revealed.

The computed activation parameters complied with the compensation effect. Two regimes were identified, namely a low-angle and a high-angle [0 0 1] twist GB regime. For the low-angle GBs, the compensation temperature was in the range of the melting temperature while for the high-angle GBs it was close to the structural transition temperature observed for both GB migration and GB self-diffusion.

Acknowledgements

The authors wish to express their gratitude to the Deutsche Forschungsgemeinschaft for financial support (Az.Go335/10). Finally we would like to thank Dr. D.A. Molodov for helpful discussions.

References

[1] Read WT, Shockley W. Phys Rev 1950;78:275–89.
[2] Molodov DA. Habilitationsschrift, Migration of high-angle grain boundaries in metals. Fakultät für Bergbau, Hüttenwesen und Geowissenschaften, Institut für Metallkunde und Metallphysik. RWTH Aachen: Shaker Verlag; 1999.
[3] Gottstein G, Shvindlerman LS. Interface Sci 1998;6: 265–76.
[4] Keblinski P, Wolf D, Phillpot SR, Gleiter H. Philos Mag A 1999;79:2735–61.
[5] Rickman JM, Phillpot SR, Wolf D, Woodraska DL, Yip S. J Mater Res 1991;6:2291–304.
[6] Bishop Jr GH, Harrison RJ, Kwok T, Yip S. J Appl Phys 1982;53:5596–608.
[7] Bishop Jr GH, Harrison RJ, Kwok T, Yip S. J Appl Phys 1982;53:5609–16.
[8] Bishop Jr GH, Harrison RJ, Kwok T, Yip S. Simulation of grain boundaries at elevated temperatures by computer molecular dynamics. In: Christian JW, Haasen P, Massalski TB, editors. Progress in materials science, Chalmers Anniversary Volume. New York: Pergamon Press; 1981. p. 49–95.
[9] Babcock SE, Balluffi RW. Acta Metall 1989;37:2367–76.
[10] Re-Jhen Jhan, Bristowe PD. Scripta Metall Mater 1990;24:1313–8.
[11] Majid I, Bristowe PD. Scripta Metall 1987;21:1153.
[12] Gottstein G, Shvindlerman LS. Grain boundary migration in metals: thermodynamics, kinetics, applications. Boca Raton, FL: CRC Press; 1999.
[13] Molodov DA, Swiderski J, Gottstein G, Lojkowski W, Shvindlerman LS. Acta Metall Mater 1994;42:3397–407.
[14] Upmanyu M, Smith RW, Srolovitz DJ. Interface Sci 1998;6:41–58.
[15] Upmanyu M, Srolovitz DJ, Shvindlerman LS, Gottstein G. Acta Mater 1999;47:3901–14.
[16] Upmanyu M, Srolovitz DJ, Shvindlerman LS, Gottstein G. Interface Sci 1998;6:287–98.
[17] Schönfelder B, Wolf D, Phillpot SR, Furtkamp M. Interface Sci 1997;5:245–62.
[18] Schönfelder B, Gottstein G, Shvindlerman LS. Met Mat Trans A, 2004, submitted for publilcation.
[19] Adler BJ, Wainwright TE. J Chem Phys 1959;31:459.
[20] Allen MP, Tildesley DJ. Computer Simulation of Liquids. New York: Clarendon Press; 1989.
[21] Nose S. Molec Phys 1986;57:187–91.
[22] Wolf D. Acta Metall 1989;37:1983–93.
[23] Wolf D. In: Wolf D, Yip S, editors. Materials interfaces: atomic-level structure, properties. New York: Chapman and Hall; 1992. [chapter 3].
[24] Rickman JM, Phillpot SR. Phys Rev Lett 1991;66:349.
[25] Jaszczak JA, Wolf D. Phys Rev B 1992;46:2473–80.
[26] Clarke AS, Jonsson H. Phys Rev E 1993;47:3975.
[27] Faken D, Jonsson H. Comp Mater Sci 1994;2:279.
[28] Phillpot SR, Lutsko JF, Wolf D, Yip S. Phys Rev B 1989;40:2831–40.
[29] Plimpton SJ, Wolf ED. Phys Rev B 1990;41:2712–21.
[30] Nomura M, Adams JB. J Mater Res 1992;7:3202–12.
[31] Winning M. Z Metallk 2004;95:233–8.
[32] Doyama M, Kogure Y. Comp Mater Sci 1999;14:80–3.
[33] Zieba P, Gust W. Interface Sci 2002;10:27–30.
[34] Zieba P. Interface Science 2003;11:51–8.
[35] Merkle KL, Thompson LJ. Interface Sci 2004;12: 277–92.